applied sciences

MDPI

Article

Method and Application of Spillway Radial Gate Vibration Signal Denoising on Multiverse Optimization Algorithm-Optimized Variational Mode Decomposition Combined with Wavelet Threshold Denoising

Xiudi Lu [1], Yakun Liu [2,*], Shoulin Tan [1], Di Zhang [2], Chen Wang [2] and Xueyu Zheng [1]

[1] Power China Guiyang Engineering Corporation Limited, Guiyang 550081, China; djgylxd@yeah.net (X.L.); zgdjtansl@163.com (S.T.); gyzhengxueyu@163.com (X.Z.)
[2] School of Infrastructure Engineering, Dalian University of Technology, Dalian 116024, China; di.zhang@dlut.edu.cn (D.Z.); wch@mail.dlut.edu.cn (C.W.)
* Correspondence: liuyakun@dlut.edu.cn

Abstract: To address the noise issue in the measured vibration signals of spillway radial gate discharge, this paper utilizes the Multiverse Optimization Algorithm (MVO) to optimize the number of decomposition modes (K) and the penalty factor (α) in Variational Mode Decomposition (VMD). This approach ensures improved efficiency of VMD decomposition while maintaining accuracy. Subsequently, the obtained Intrinsic Mode Functions (IMFs) from VMD decomposition are classified based on Multi-scale Permutation Entropy (MPE). IMFs are divided into pure components and noisy components; the noisy components are processed with Wavelet Threshold Denoising (WTD), while the pure components are overlaid and reconstructed to obtain the denoised vibration signal of the gate. Comprehensive comparisons involving artificial signal simulations, gate flow-induced vibration model tests, and numerical simulations lead to the following conclusions: compared to other algorithms, the proposed combined denoising method (MVO-VMD-MPE-WTD) achieves the highest signal-to-noise ratio (SNR) in both the frequency and time domains for artificial signals, while yielding the lowest mean square error (MSE). In the gate flow-induced vibration model tests, the method significantly reduces noise in the vibration signals and effectively preserves characteristic information. The error in preserving characteristic information across model tests and numerical simulations is kept below 1%. Furthermore, compared to other optimization algorithms, the MVO demonstrates higher computational efficiency. The parameter-optimized combined denoising method proposed in this study provides insights into denoising measured vibration signals of hydraulic spillway radial gates and other drainage structures, and it opens possibilities for exploring more efficient optimization algorithms for achieving online monitoring in the future.

Keywords: spillway radial gate; vibration noise; VMD; joint denoising; numerical simulation

Citation: Lu, X.; Liu, Y.; Tan, S.; Zhang, D.; Wang, C.; Zheng, X. Method and Application of Spillway Radial Gate Vibration Signal Denoising on Multiverse Optimization Algorithm-Optimized Variational Mode Decomposition Combined with Wavelet Threshold Denoising. *Appl. Sci.* **2024**, *14*, 9650. https://doi.org/10.3390/app14219650

Academic Editor: Tomasz Figlus

Received: 12 September 2024
Revised: 11 October 2024
Accepted: 17 October 2024
Published: 22 October 2024

1. Introduction

A spillway radial gate (SRG), as a critical drainage structure, is widely used as a dam discharge gate due to its advantages, such as the absence of gate slots and favorable downstream flow conditions. During power generation and flood discharge operations, the SRG must be opened and closed in a timely manner to control flow, making its safe operation crucial to both dam efficiency and the safety of downstream lives and property [1,2]. The SRG primarily bears loads on its panel, which are then distributed by horizontal and vertical beams, and finally transferred to the pier through supporting arms. However, accident investigations have revealed that SRGs often fail due to instability in the supporting arms. In addition to intrinsic factors like water flow excitation and the structure's natural frequencies, fatigue and corrosion are also significant causes of arm instability [3,4]. As

such, real-time or periodic safety monitoring of the gate is essential. Installing sensors on the gate for prototype observation is one of the most direct and commonly used methods to assess gate conditions or analyze the causes of vibration [5]. Gate vibrations involve several complex nonlinear issues, including material nonlinearity and contact nonlinearity, which exhibit chaotic characteristics in the vibration signals. Moreover, the harsh and complex operational environment of the gate results in sensor-measured signals often containing noise, which introduces disturbances during further processing. For instance, noise can lead to false modal identification during a modal parameter analysis and reduce efficiency in condition monitoring [6].

Traditional noise reduction methods, such as mean and median filtering, rely on statistical principles, using local signal characteristics to remove noise. However, these methods are often limited when dealing with non-stationary signals or when noise characteristics vary significantly. Additionally, they require sufficient sample data for an effective analysis. Recently, with the development of non-stationary signal processing techniques, methods like Empirical Mode Decomposition (EMD) [7], Variational Mode Decomposition (VMD) [8], and Wavelet Threshold Denoising (WTD) offer a multiscale analysis to effectively remove noise across various frequency ranges [9]. EMD is suitable for processing nonlinear and non-stationary time series but faces challenges like mode mixing, sensitivity to parameter settings, and end effects, making the separation of characteristic frequencies and noise in signals less accurate. In comparison, VMD provides better robustness in sampling and noise suppression, effectively reducing mode mixing and achieving more precise decomposition results. However, VMD is sensitive to the number of decomposition modes (K) and the penalty factor (α), which can lead to over-decomposition or under-decomposition [10]. Too few modes may miss important signal features, while too many modes may introduce unnecessary noise or patterns. A larger penalty factor (α) results in smoother solutions, potentially losing signal details, whereas a smaller penalty factor may lead to non-smooth solutions or even oscillations. With advances in mathematical optimization, optimizing VMD parameters can enhance accuracy, reduce subjectivity in parameter selection, and improve computational efficiency. This enables a more effective handling and analysis of complex signals, laying a solid foundation for further signal processing and feature extraction. Numerous researchers [11–15] have studied the selection and application of VMD parameters (K and α). Yan [14] proposed an improved cuckoo search algorithm to optimize VMD, demonstrating its accuracy through experiments and simulations. Wang [15] used the whale optimization algorithm to adaptively determine VMD parameters, improving the efficiency of a bearing fault diagnosis.

Multiscale Permutation Entropy (MPE) is a statistical tool for analyzing the complexity and nonlinearity of time series through a multiscale analysis [16,17]. It reveals dynamic data behavior at different scales and is widely applied in signal processing. An MPE threshold of 0.6 distinguishes between noisy and clean components. IMF components with an MPE greater than 0.6 are considered noisy, while those below 0.6 are considered clean [18]. This paper addresses the challenge of manually selecting K and α in traditional VMD, which can reduce decomposition effectiveness. Given the large volume of gate vibration data requiring robust optimization, this paper proposes the MVO-VMD-MPE-WTD joint denoising method to improve signal processing quality. The MVO algorithm optimizes the number of modes and penalty factor in VMD, achieving optimal signal decomposition. MPE is then used to assess the noise content of each IMF. Noisy components are denoised using WTD, and finally, the processed components are combined with the clean ones to complete denoising. This approach improves both decomposition accuracy and the robustness and adaptability of the algorithm. This method is applied to denoise measured vibration data from spillway gates in a hydraulic project. Prototype observations and numerical simulations jointly demonstrate the method's effectiveness.

2. Basic Theories

2.1. Multiverse Optimizer Algorithm [19]

Traditional VMD performs signal decomposition by setting decomposition parameters, which may struggle to fully optimize different objectives. By using the MVO optimization algorithm, a balance between multiple objectives can be achieved, thereby improving the accuracy of the noise reduction effect. The Multiverse Optimizer (MVO) is a population intelligence optimization algorithm proposed jointly by S. Mirjalili, S.M. Mirjalili, and A. Hatamlou in 2015, based on the multiverse theory in physics. It simulates the movement behavior of populations in a multiverse under the influences of white holes, black holes, and wormholes. The algorithm is divided into exploration and exploitation phases, where white holes and black holes operate during the exploration phase, while wormholes operate during the exploitation phase. The specific process is as follows:

The production of the initial population:

$$U = \begin{bmatrix} x_1^1 & x_1^2 & \cdots & x_1^d \\ x_2^1 & x_2^2 & \cdots & x_2^d \\ \vdots & \vdots & \vdots & \vdots \\ x_n^1 & x_n^2 & \cdots & x_n^d \end{bmatrix} \tag{1}$$

Then, according to the roulette wheel mechanism, each object in the multiverse system undergoes transitions through the trajectories of white holes and black holes. The process is expressed as follows:

$$x_i^j = \begin{cases} \begin{cases} X_j + TDR \times \left(\left(ub_j - lb_j \right) \times r4 + lb_j \right), \ r3 < 0.5 \\ X_j - TDR \times \left(\left(ub_j - lb_j \right) \times r4 + lb_j \right), \ r3 \geq 0.5 \end{cases} \\ x_i^j, \ r2 \geq WEP \end{cases} \tag{2}$$

In the equation, X_j represents the j object of the current optimal universe; lb_j and ub_j are the lower and upper bounds of x, respectively. $r2$, $r3$, and $r4$ are random numbers in the range [0, 1]. *WEP* (Wormhole Existence Probability) and *TDR* (Traveling Distance Ratio) are two important parameters, and their update principles are described by the following equations:

$$WEP = WEP_{\min} + l \times \left(\frac{WEP_{\max} - WEP_{\min}}{L} \right) \tag{3}$$

$$TDR = 1 - \frac{l^{1/p}}{L^{1/p}} \tag{4}$$

2.2. Variational Mode Decomposition [11–15]

Compared to the traditional Empirical Mode Decomposition (EMD) algorithm, Variational Mode Decomposition (VMD) is an adaptive and fully non-recursive method for mode variation and signal processing proposed by Konstantin Dragomiretskiy in 2014. Its adaptability allows for determining the number of Intrinsic Mode Function components based on the actual sequence. VMD decomposition overcomes the end-point effects and mode mixing problems of EMD decomposition. The corresponding mathematical equation is

$$u_k(t) = A_k(t) \cos(\phi_k(t)) \tag{5}$$

In the equation, $\{u_k\}$ represents the instantaneous amplitude, and $\varphi_k(t)$ represents the instantaneous phase. Through the Hilbert–Huang Transform (HHT), analytic signals of different modes are obtained. Subsequently, each Intrinsic Mode Function (IMF) signal is modulated to its corresponding baseband by multiplying with the estimated center frequency.

By applying Gaussian smoothness, the bandwidth of each IMF component is estimated to yield a constrained variational model:

$$\begin{cases} \min\limits_{\{u_k\},\{\omega_k\}} \left\{ \sum\limits_k \left\| \partial_t \left[\left(\delta(t) + \dfrac{j}{\pi t} \right) \times u_k(t) \right] e^{-j\omega_k t} \right\|^2 \right\} \\ s.t. \sum\limits_k u_k = f \end{cases} \tag{6}$$

In the equation, $\{u_k\}$ represents the K IMFs of the decomposition, $\{\omega_k\}$ denotes the central frequency component of each IMF, and f is the input signal.

To find the optimal solution for the constrained variational problem, the Lagrange multiplier τ(t) and a second-order penalty factor (α) are introduced to transform the constrained variational problem into an unconstrained variational problem. The τ(t) ensures the strictness of the constraints, while the α ensures accurate signal reconstruction in Gaussian noise environments. The extended Lagrangian expression is as follows:

$$\begin{aligned} L(\{u_k\},\{\omega_k\},\lambda) = \alpha \sum_k \left\| \partial_t \left[\left(\delta(t) + \frac{j}{\pi t} \right) \times u_k(t) \right] e^{-j\omega_k t} \right\|^2 + \left\| f(t) - \sum_k u_k(t) \right\|_2^2 \\ + \left\langle \lambda(t), f(t) - \sum_k u_k(t) \right\rangle \end{aligned} \tag{7}$$

Then, utilizing the Alternating Direction Method of Multipliers (ADMM), we make a succession update of each component and central frequency to obtain the saddle point of the unconstrained model. Based on frequency-domain space, all components are derived as follows:

$$\hat{u}_k^{n+1}(\omega) = \frac{\hat{f}(\omega) - \sum_{i \neq k} \hat{u}_i(\omega) + \dfrac{\hat{\lambda}(\omega)}{2}}{1 + 2\alpha(\omega - \omega_k)^2} \tag{8}$$

$$\begin{cases} \min\limits_{\{u_k\},\{\omega_k\}} \left\{ \sum\limits_k \left\| \partial_t \left[\left(\delta(t) + \dfrac{j}{\pi t} \right) \times u_k(t) \right] e^{-j\omega_k t} \right\|^2 \right\} \\ s.t. \sum\limits_k u_k = f \end{cases} \tag{9}$$

2.3. Multiscale Permutation Entropy [18]

Permutation Entropy (PE) is a measure method of complexity based on symbolic representation. The main idea is to reconstruct a time series into a symbolic sequence and then compute the entropy of this sequence. Multiscale Permutation Entropy (MPE) extends the concept of PE by incorporating multiscale processes, allowing the analysis of dynamic features of time series across different scales. MPE can be used to evaluate the complexity and randomness of signals, helping to identify which modal components might contain more noise. By quantifying the entropy values of each mode, MPE further enhances the ability to distinguish between noise and signal characteristics. The specific steps of MPE are as follows:

(1) Multiscale Process: Construct multiscale time series by coarse-graining the original time series. Given a time series $\{x_i\}_{i=1}^N$ and a scale factor (s), construct the coarse-grained time series as follows:

$$y_j^{(s)} = \frac{1}{s} \sum_{i=(j-1)s+1}^{js} x_i, j = 1, 2, \ldots, \left[\frac{N}{s} \right] \tag{10}$$

(2) Calculate the Permutation Entropy at different scales: For each scale (s), calculate the $PE(s)$ of the coarse-grained time series $\left\{ y_j^{(s)} \right\}$, and then follow the standard procedure for Permutation Entropy.

(3) MPE is defined as the collection of permutation entropies at different scales:

$$MPE = \{ PE(s) | s = 1, 2, \ldots, S \} \tag{11}$$

In the equation, S is the maximum scale factor.

2.4. MVO-VMD-MPE-WTD Flowchart

In summary, this paper proposes a combined denoising method based on the optimization of VMD using MVO, coupled with MPE and WTD, referred to as MVO-VMD-MPE-WTD. Compared to traditional single denoising methods such as VMD decomposition or WTD, the proposed combined method offers significant advantages. Traditional VMD decomposes the signal by setting decomposition parameters, which may not fully account for the optimization of multiple objectives. In contrast, the MVO algorithm optimizes the decomposition parameters of VMD to enable the extracted modes to more accurately represent the characteristic patterns of the original signal. Meanwhile, MPE can quantify the entropy values of each mode to assess signal complexity and randomness, to identify which modal components may contain more noise. This further improves the ability to distinguish between noise and signal characteristics.

WTD, as an effective tool for processing non-stationary signals, when combined with VMD and MPE, allows for more refined multiscale signal processing in the time–frequency domain, thereby enhancing denoising performance. Specifically, the MVO-VMD-MPE-WTD method demonstrates stronger adaptability and noise reduction capability, effectively removing noise while retaining more useful signal characteristics. The flowchart of the combined denoising process is shown in Figure 1.

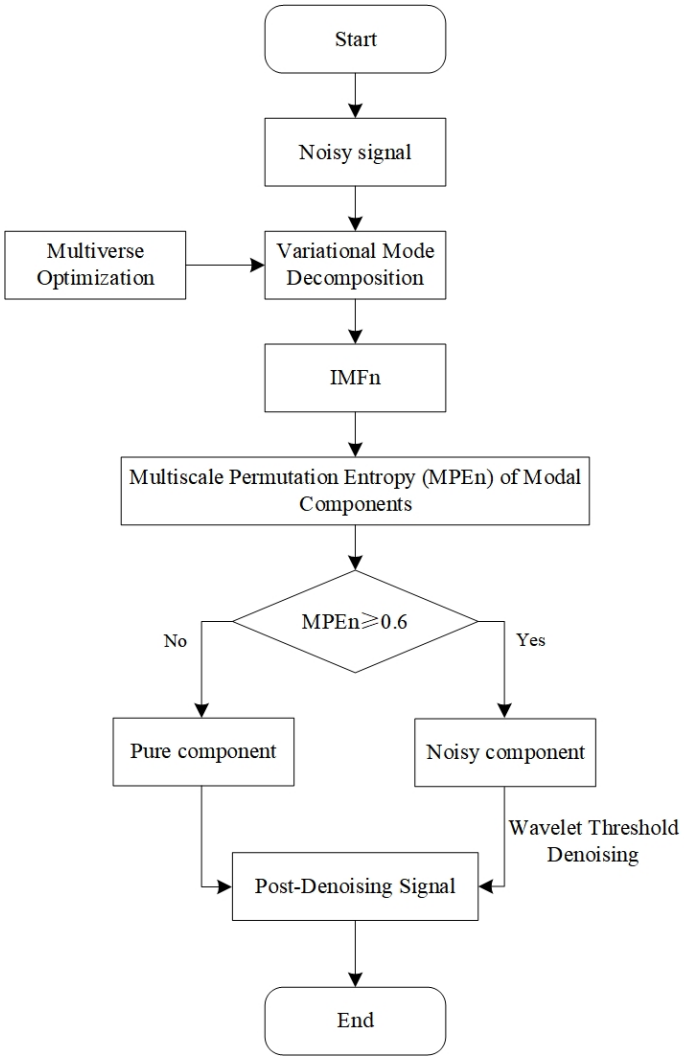

Figure 1. Flowchart of MVO-VMD-MPE-WTD.

3. Artificial Simulation Signal Denoising

To evaluate the performance of the denoising algorithm proposed in this paper, we first verify the effectiveness of the denoising method (MVO-VMD-MPE-WTD) using artificially simulated signals. Let

$$\begin{cases} Y = X_1 + X_2 + X_3 + X_{noise} \\ X_1 = \cos(\pi t) \\ X_2 = 2\sin(2\pi t) \\ X_3 = 4\cos(8\pi t) \\ X_{noise} = 2randn(N, 1) \end{cases} \tag{12}$$

In the equation, X_1, X_2, and X_3 are three pure signals with different frequencies; X_{noise} is a random white noise signal; and Y is the noisy simulation signal. The waveforms of the pure signals, noisy signals, and denoised signals obtained using the proposed denoising method are compared as shown in Figure 2.

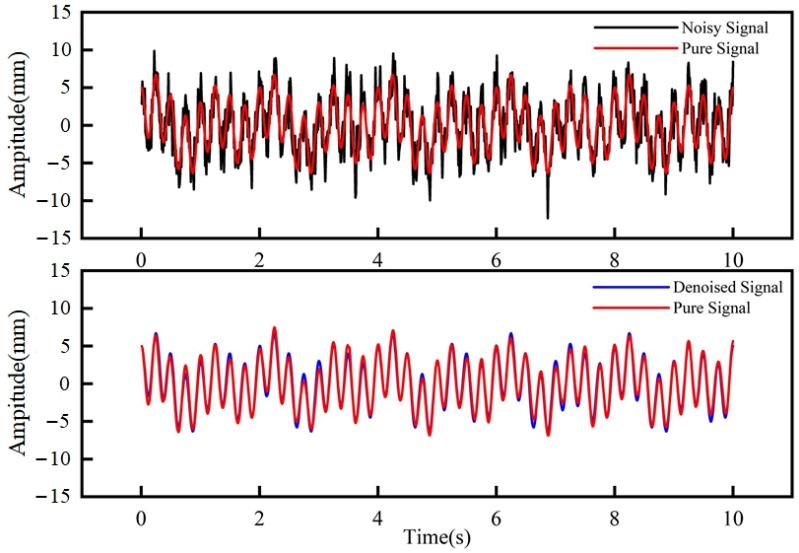

Figure 2. Comparison of denoising results for artificial signals.

From the comparison of the denoising results, it is clear that after noise is added to the original signal, its trend becomes irregular. Noise completely obscures the original signal, which makes it difficult to distinguish the original waveform. After applying the proposed denoising method, the denoised signal closely matches the waveform of the original signal.

To quantitatively compare the effectiveness of the denoising algorithm, we analyze the signal-to-noise ratio (*SNR*) and mean squared error (*MSE*) before and after denoising. *SNR* is a crucial indicator of signal quality; a higher *SNR* means less noise in the signal. *MSE* reflects the average squared error between the original and denoised signals; a lower *MSE* indicates better denoising performance [20–22]. To further verify the accuracy of the *SNR* evaluation trend, both frequency-domain *SNR* and time-domain *SNR* are introduced. The calculation formulas for frequency-domain *SNR*, time-domain *SNR*, and *MSE* are as follows:

$$SNR_{time} = 10\ \log_{10}\left(\frac{\sum_{n=1}^{N} s[n]^2}{\sum_{n=1}^{N} n[n]^2}\right) \tag{13}$$

$$SNR_{freq} = 10\ \log_{10}\left(\frac{\sum_{n=1}^{N} |X[k]|^2}{\sum_{n=1}^{N} |N[k]|^2}\right) \tag{14}$$

$$MSE = \frac{1}{N}\sum_{i=1}^{N}(x_i - \hat{x}_i)^2 \tag{15}$$

In these equations, SNR_{time} represents the signal-to-noise ratio in the time domain, and SNR_{freq} represents the signal-to-noise ratio in the frequency domain. $X[k]$ denotes the FFT (Fast Fourier Transform) result of the signal at the k-th frequency component, and $N[k]$ represents the FFT result of the noise at the k-th frequency component. $s[n]$ is the signal value at the n-th time point, and $n[n]$ is the noise value at the n-th time point.

Using the proposed method for denoising artificial signals, it is found that the optimal number of VMD decomposition layers is 12. To further highlight the effectiveness of this algorithm, instead of optimizing the VMD decomposition layers with MVO, we manually set the VMD decomposition layers to 5–11 and 13–14, resulting in the VMD-MPE-WTD algorithm (K = 5, 6, 7, 8, 9, 10, 11, 13, 14). Additionally, we include a comparison with wavelet thresholding denoising (WTD) to emphasize the benefits of joint decomposition and denoising. The results of various denoising methods are compared in Table 1.

Table 1. Quantitative Metrics of Denoising Methods.

	SNR_{time}	SNR_{freq}	*MSE*
WTD	8.113	8.4234	1.5107
VMD-MPE-WTD (K = 5)	13.9798	14.0333	0.76906
VMD-MPE-WTD (K = 6)	14.2041	14.0708	0.74944
VMD-MPE-WTD (K = 7)	14.2582	14.5762	0.7448
VMD-MPE-WTD (K = 8)	15.3158	14.8874	0.65941
VMD-MPE-WTD (K = 9)	14.7305	14.818	0.70538
VMD-MPE-WTD (K = 10)	15.0113	16.1797	0.68294
VMD-MPE-WTD (K = 11)	16.05	15.4067	0.60596
MVO-VMD-MPE-WTD	16.3866	17.4829	0.58293
VMD-MPE-WTD (K = 13)	15.5514	16.7632	0.64176
VMD-MPE-WTD (K = 14)	16.1047	16.9452	0.60216

Based on the calculations, it is observed that the time-domain *SNR* of the original noisy signal is 5.7327, while the frequency-domain *SNR* is 5.6694. All denoising methods improve the *SNR* of the noisy signals to some extent. The joint denoising method shows a significant enhancement in performance compared to the single WTD denoising method. There is no clear correlation between the number of decomposition layers and denoising effectiveness, since an increase in the number of layers may either improve or worsen the denoising results. However, among all results, the decomposition with 12 layers optimized by MVO provides the best results. Since the frequency-domain *SNR* and time-domain *SNR* are computed in different representation domains, the frequency-domain *SNR* may be affected by factors such as the selection of sampling frequency windows during the FFT process, leading to certain discrepancies between the two. However, overall, both exhibit the same evaluation trend.

In summary, the proposed method achieves the highest *SNR* and the lowest MSR for denoising artificial simulated signals. It allows for an adaptive optimization of VMD decomposition parameters to avoid the influence of manually selected parameters on the results, thereby enhancing both denoising accuracy and efficiency.

4. Model Testing of Actual Signal Denoising

4.1. Project Overview

The BDa Hydropower Station is a large-scale hydraulic project located in southwestern China. This paper studies the spillway radial gate used in the ecological spillway section of the dam. This section features a roller-compacted concrete gravity dam, and the spillway radial gate employs a straight cantilever and main longitudinal beam frame structure. Due to ecological flow requirements, the gate needs to operate for extended periods at small openings. To assess the vibration behavior of the gate under these conditions, a feasibility analysis of flow-induced vibrations is necessary.

Flow-induced vibrations of the gate fall under the category of hydroelastic vibrations. The operation under flowing water is governed by the following dynamic equation,

$$[M]\left\{\ddot{D}\right\} + [C]\left\{\dot{D}\right\} + [K] = \{F_1\} + \{F_2\} \quad (16)$$

In the equation, $[M]$ represents the mass matrix, $[C]$ represents the damping matrix, and $[K]$ represents the stiffness matrix. $\left\{\ddot{D}\right\}$ denotes the acceleration vector, $\left\{\dot{D}\right\}$ denotes the velocity vector, and $\{D\}$ denotes the displacement vector of the nodes. $\{F\}$ represents the dynamic water pressure vector acting on the fluid–structure interaction interface nodes.$\{F_1\}$ represents the water flow load vectoracting on the gate when it is ina'stationarystate and the additionalload. $\{F_2\}$ is the disturbed flow field resulting from gate vibrations.

4.2. Model Testing

The main material of the gate for this project is Q345C structural steel, with an elastic modulus (E) of 200 GPa, a unit weight of 78.5 kN/m³, and a Poisson's ratio of 0.3. According to hydroelastic similarity principles, the primary material for the hydroelastic simulation consists of heavy metal tungsten powder mixed with epoxy resin, reinforcing materials, curing agents, and diluents. This polymer composite, produced by the State Key Laboratory of Hydraulic Engineering Simulation and Safety at Tianjin University, has an elastic modulus of 8 GPa. In the hydroelastic vibration model, the fluid motion and structural vibrations maintain geometric, kinematic, and dynamic similarity with the prototype. The flow-induced vibration experiments are conducted at the Hydraulic Laboratory of Dalian University of Technology, where acceleration measurements are taken at typical points during the gate's discharge process. The primary focus is on measuring the acceleration at typical measurement points during the gate discharge process. Multiple tri-axial accelerometers are installed on the upper and lower arms of the gate to monitor the acceleration response under discharge conditions. The water flow excites the gate, causing vibrations, and the accelerometers collect acceleration data from the measurement points, which are then transmitted to the data acquisition system via cables. The layout of the measurement points for the gate flow-induced vibration test and the discharge data collection process is shown in Figure 3.

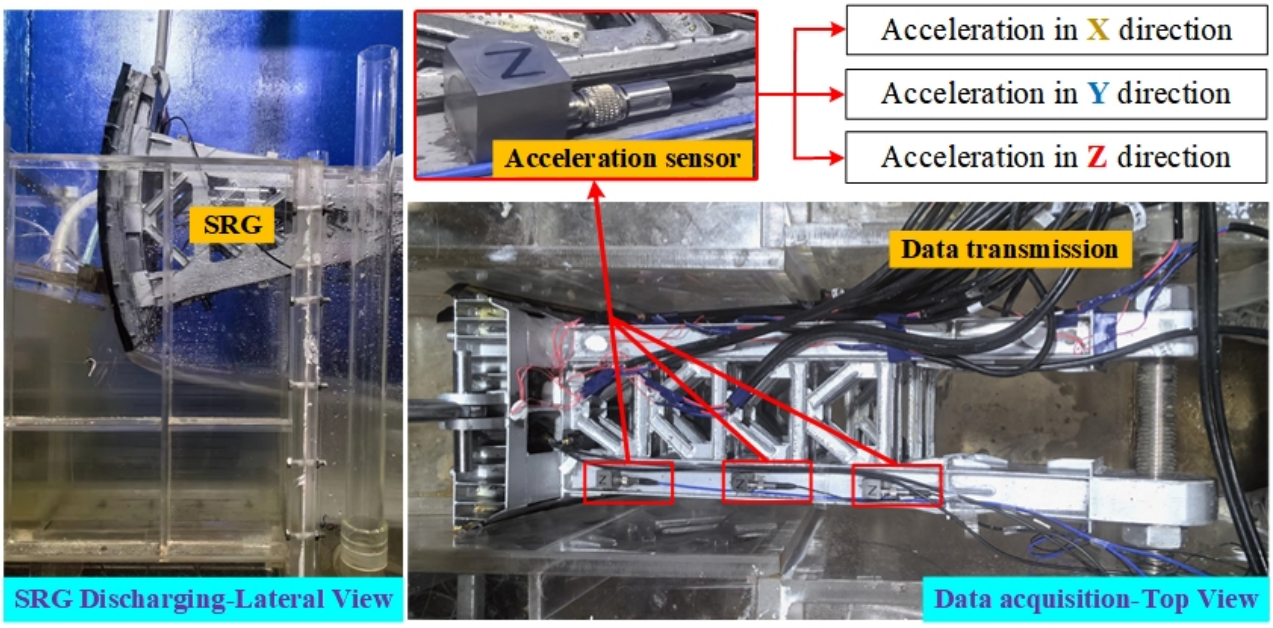

Figure 3. Flow-induced vibration model test.

4.3. Signal Denoising Processing

A further analysis requires denoising the obtained vibration acceleration signals. Due to space constraints, this section presents results using the z-direction acceleration of the sensor at the front end of the lower arm when the ecological discharge is at 20% of opening. Acceleration time-history data from each channel show that the measured vibration signals contain significant noise, with multiple spikes in the curves.

When denoising the measured vibration signals using the method described in this paper, the VMD parameters are first adaptively optimized based on the MVO algorithm. The MVO-VMD-MPE-WTD iterative optimization curve is shown in Figure 4. From Figure 4, it can be determined that the optimal number of VMD modes is K = 12 and the secondary penalty factor is α = 2000.

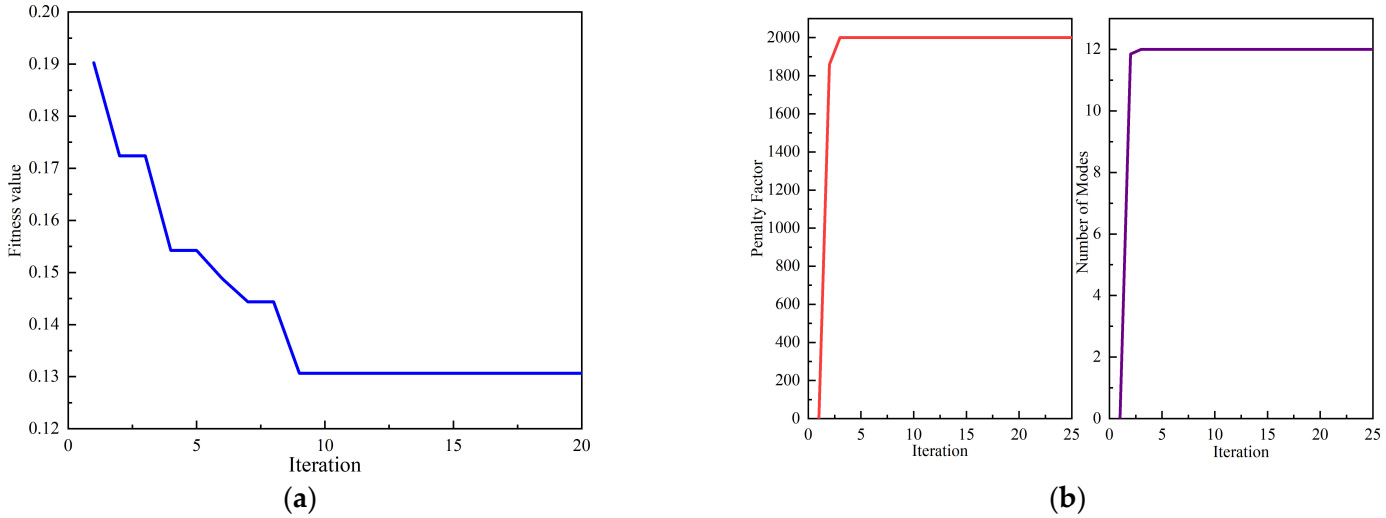

Figure 4. MVO-VMD-MPE-WTD convergence curve: (**a**) MVO-VMD adaptive curve; (**b**) VMD convergence curve.

The MVO-optimized VMD decomposition results are shown in Figure 5.

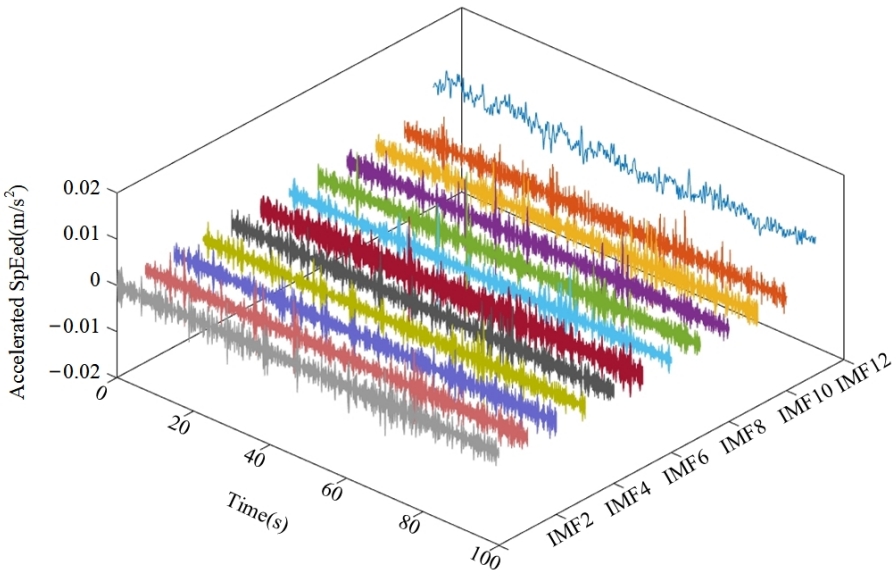

Figure 5. MVO-VMD-MPE-WTD decomposition results.

Based on the VMD decomposition results, the original signal is decomposed into 12 IMF components. The MPE values for each IMF component are calculated and displayed in Figure 6.

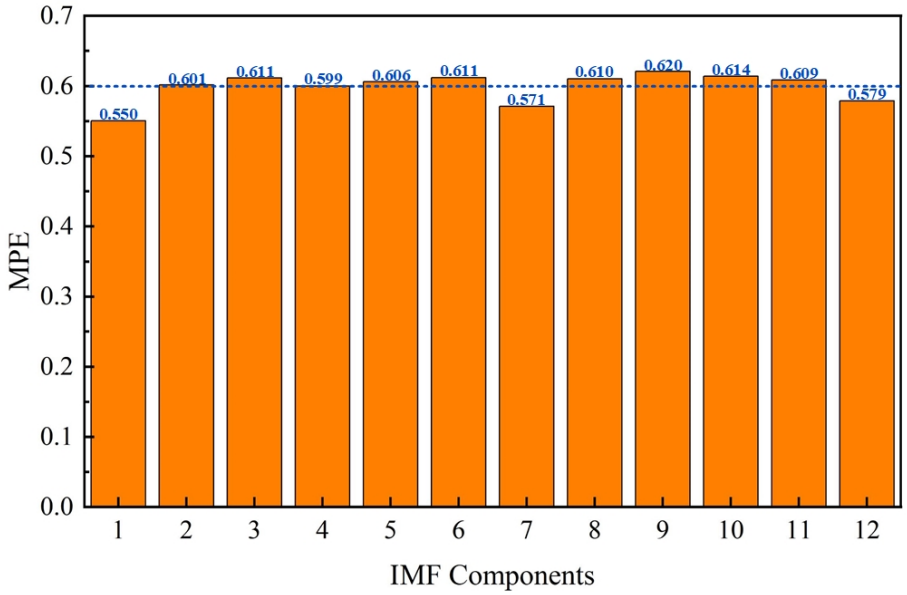

Figure 6. MPE of each IMF component.

According to Figure 6, among the 12 IMF components obtained from VMD decomposition, the MPE values of the 1st, 4th, 7th, and 12th components are less than 0.6 and are considered pure components. The remaining IMF components are regarded as noise and need to be denoised using wavelet thresholding. The db4 wavelet is used as the basis function, and a hard threshold is applied. After denoising the noise components, they are then combined with the pure components and reconstructed to obtain the denoised vibration signal. The comparison of the signal before and after denoising is shown in Figure 7.

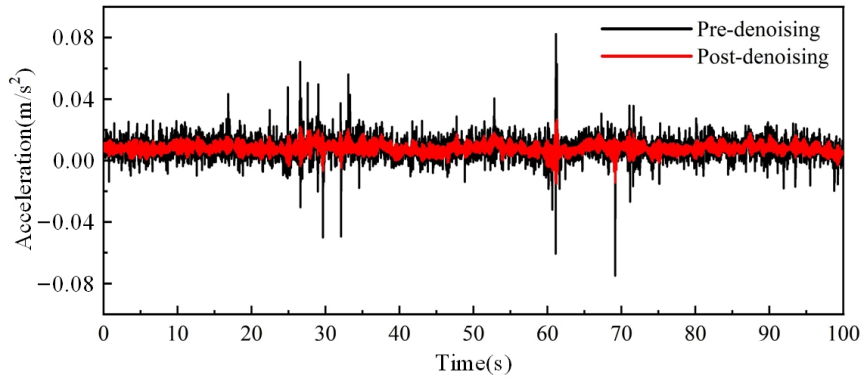

Figure 7. Comparison of signals on pre-denoising and post-denoising.

In practical engineering, the power of both the useful signal and noise in the measured signal is unknown, making it impossible to assess denoising performance using *SNR*. Therefore, this paper introduces the d_{nSNR} [23] to quantitatively evaluate the quality of denoising, with the calculation formula as follows:

$$d_{nSNR} = 10 \log_{10}(P_s/P_g) \quad (17)$$

In the equation, P_s represents the power of the noisy signal; P_g represents the power of the denoised signal.

When denoising the measured signal, three approaches are used: Experimental Group A only uses WTD for denoising; Group B discards noise components directly after MVO-VMD-MPE decomposition; and the control group uses the method described in this paper for denoising. The d_{nSNR} results for each method are shown in Table 2:

Table 2. d_{nSNR} Results for Each Method.

Denoising Methods	d_{nSNR}
WTD	6.6242
MVO-VMD-MPE (Discarding Noise IMF)	3.9179
MVO-VMD-MPE-WTD	1.14

According to the calculation results, the MVO-VMD-MPE-WTD method achieves the lowest dnSNR value of 1.14, demonstrating superior performance compared to the other two denoising methods. The combination of MVO-optimized VMD decomposition and WTD offers the best denoising performance. Based on d_{nSNR}, the method proposed in this paper results in the smallest error and the most effective denoising of the measured signal from the spillway radial gate.

4.4. Comparison of Optimization Algorithms

With the advancement in mathematical theories, various optimization algorithms have emerged. To highlight the advantages of the MVO optimization algorithm, we compare it with the NGO, AOA, and RIME [24,25] optimization methods. The calculation results are shown in Table 3.

Table 3. Comparison of Optimization Algorithms.

	K	α	Computation Time (s)
NGO	12	2000	1180.2
AOA	12	2000	1266.6
MVO	12	2000	1113.3
RIME	12	2000	1421.1

According to the table, when optimizing the VMD hyperparameters with the four optimization methods, the penalty factor α converges at 2000 for all methods, and the optimal number of modes for each method is 12. All four methods can be used for optimizing VMD decomposition hyperparameters. However, in terms of computation time comparison, the MVO optimization method presented in this paper has the shortest computation time and the highest efficiency for gate vibration signals.

5. Accuracy Verification of Denoising Data

To verify the accuracy of the denoising algorithm proposed in this paper, ensuring that noise is effectively removed while preserving the main components of the original signal, sensor-acquired signals are directly fused based on variance contribution rates as the control group. For the experimental group, the sensor-acquired signals are first denoised using the proposed method, then fused based on the same variance contribution rates [26,27]. Both groups are subjected to a spectral analysis to examine the prominent frequencies of the denoised signals.

The data fusion method, based on the variance contribution rate of correlation, allocates fusion coefficients according to the importance of the correlation between information, enabling a dynamic fusion of similar data. This approach consolidates multiple similar signals into a single signal.

For the data point x_{ij} from the (j)-th point of the (i)-th sensor, the equation for the variance contribution rate of these data is

$$K_{ij} = \frac{(x_{ij} - E_i)^2}{m\sigma_i^2} \tag{18}$$

Here, m is the number of data points, E is the mean of the data sequence, and σ^2 is the variance of the data sequence.

Based on the variance contribution rate of similar signals collected from m channels at a given time, the allocation coefficient K_{ij} for any sensor signal x_i is

$$k_{ij} = \frac{K_{ij}}{\sum_{i=1}^{m} K_{ij}} \tag{19}$$

Based on the obtained allocation coefficients, the signals collected from m channels can be fused into a single signal. After fusion, the value (x) of the (j)-th data point from the (x)-th channel is

$$x = \sum_{i=1}^{m} k_{ij} x_{ij} \tag{20}$$

The normalized power spectral density curves for the control group and the experimental group are shown in Figure 8.

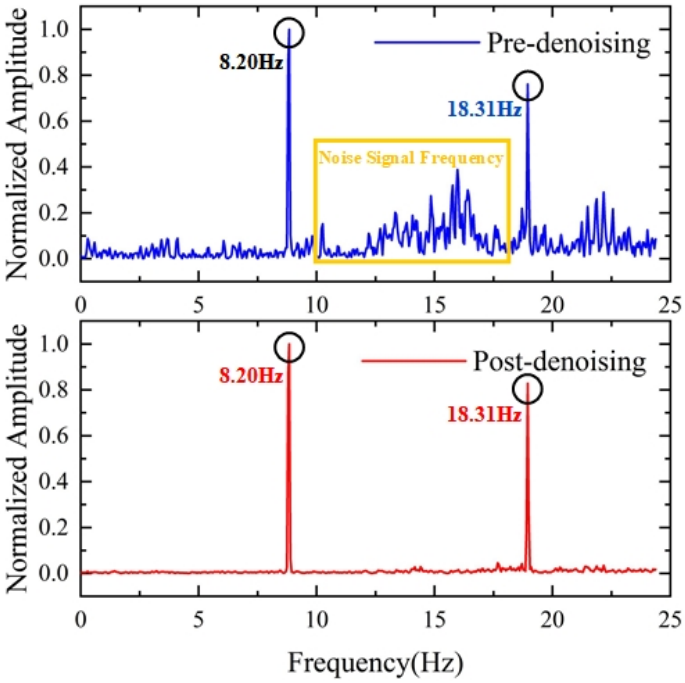

Figure 8. Comparison of normalized power spectral density curves on pre-denoising and post-denoising.

In the evaluation of self-excited vibrations, the dominant frequency has a significant impact on the stability of the system. By comparing the FFT transformations before and after denoising, it can be observed that the noise frequencies have been effectively eliminated, making the dominant frequency more prominent. From the comparison of normalized power spectral density curves before and after denoising, it can be observed that the frequency of peak point 1 is 8.20 Hz and the frequency of peak point 2 is 18.31 Hz. Denoising effectively removes noise and makes the signal peaks more pronounced.

To further validate the effectiveness of denoising in preserving key information, a numerical simulation is performed for the measurement with a 20% gate opening. This

simulation demonstrates the validity of the key information from a numerical perspective. The gate–water coupling model is shown in Figure 9.

Rotational degrees of freedom are applied at the gate lifting lug to simulate the rotational effect of the opening and closing rod bearings. Similarly, rotational degrees of freedom are applied at the hinge plate to simulate the gate's rotation around the lifting lug axis [28,29]. The water body is modeled using Fluid30 elements, and the gate is modeled with Shell181 shell elements [30–33]. The first and second-order natural frequencies are shown in Figure 10.

According to the natural frequencies, the first- and second-order modes of the gate show vibrations in the flow direction, with the gate panel divided symmetrically. The first-order natural frequency is 8.27 Hz, and the second-order natural frequency is 18.20 Hz. The numerical simulation frequencies match the peak power points in Figure 6, with an error of no more than 1%. This demonstrates that the method used in this paper effectively preserves the main information of the signal after denoising, as confirmed by numerical results in practical hydraulic engineering projects.

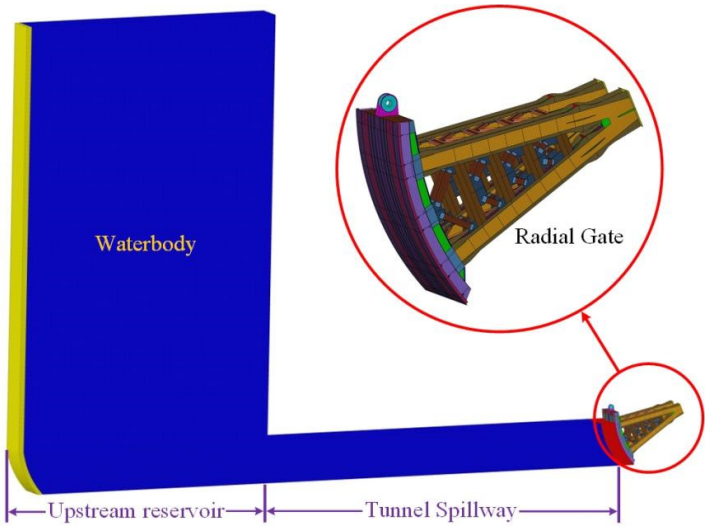

Figure 9. Finite element model of gate–structure coupling.

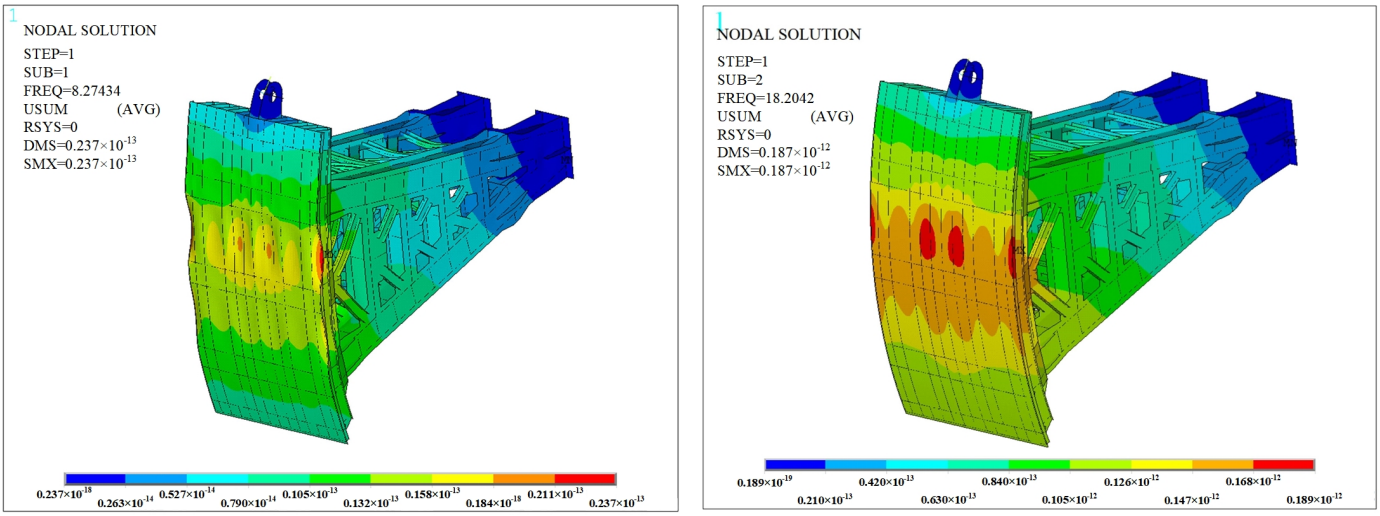

(**a**) (**b**)

Figure 10. Contout plots: (**a**) wet-mode-shape contour plot of the first-order; (**b**) wet-mode-shape contour plot of the second order.

6. Results and Discussion

The proposed MVO-optimized VMD method combined with Wavelet Threshold Denoising (WTD) demonstrates superior performance in both simulated and real-world denoising tasks regarding vibration signals. The results are discussed in detail below:

(1) Verification of Noise Reduction Performance

In the simulation experiments, the proposed method significantly enhances the signal-to-noise ratio (SNR) and reduces the mean square error (MSE). Specifically, the SNR of the noisy signal increases from 5.7327 to 16.3866, while the MSE decreases to 0.58293. In contrast, the standalone Wavelet Threshold Denoising method yields an SNR of 8.113 and an MSE of 1.5107, indicating that the MVO-VMD-MPE-WTD approach outperformed traditional methods. Additionally, a comparison of different decomposition levels (e.g., SNR of 13.9798 for K = 5 vs. 16.3866 for K = 12) shows that the MVO-optimized decomposition level of 12 provided the best noise reduction results, further validating the efficacy of the proposed method.

(2) Effectiveness of Adaptive Parameter Optimization

The selection of the number of modes (K) and penalty factor (α) is critical in traditional VMD. If the choice is inappropriate, it can easily lead to excessive or insufficient signal decomposition. By utilizing the MVO algorithm to adaptively optimize these parameters, the proposed method avoids the subjectivity of manual selection and enhances the precision and efficiency of signal decomposition. The experimental results indicate that, for the case study in this paper, the optimal number of decomposition levels is 12 and the penalty factor α is 2000, demonstrating that this parameter combination can minimize noise while preserving the key characteristics of the signal.

(3) Comparison with Other Optimization Algorithms

To assess the superiority of the MVO algorithm, it is compared with other optimization methods such as NGO and AOA. Although all algorithms successfully optimized VMD parameters, MVO demonstrates greater computational efficiency and noise reduction performance. For instance, MVO required 1113.3 s of computation time, which is significantly lower than NGO (1180.2 s) and AOA (1266.6 s). Furthermore, the noise reduction error ratio of the MVO-VMD-MPE-WTD method is 1.14, considerably better than the standalone Wavelet Threshold Denoising method (6.6242) and the MVO-VMD method that discards noisy IMFs (3.9179). This highlights the superior efficiency and effectiveness of the proposed method.

(4) Performance in Real Engineering Applications

In the denoising processing of flow-induced vibration measurement signals of an arcuate spillway radial gate, the proposed approach exhibited strong adaptability and robustness. The noisy signal, characterized by numerous spikes, is significantly smoothed after denoising. The power spectral density analysis shows that the main frequency peaks after denoising (8.20 Hz and 18.31 Hz) closely match the natural frequencies obtained from numerical simulation (8.27 Hz and 18.20 Hz), with an error margin of less than 1%. This result confirms that the proposed method effectively retains the essential frequency components of the signal while substantially improving signal quality.

(5) Retention of Signal Characteristics and Accuracy Validation

The analysis of power spectral density further demonstrates that the key frequency components of the signal remained stable after denoising, confirming that the proposed method not only reduces noise but also preserves critical signal features. Comparison with numerical simulation results reinforces the method's applicability in real engineering contexts, as the denoised signal accurately reflects the actual vibration characteristics, illustrating the reliability and practicality of the proposed method in handling complex signals.

7. Conclusions

1. To address the significant impact of the penalty factor and the number of decomposition layers on the results during VMD decomposition, we introduced the MVO-VMD decomposition method and further combined MPE and WDT to propose the MVO-VMD-MPE-WDT joint denoising method. This method uses MVO to optimize the decomposition layers (K) and penalty factor (α) in VMD decomposition. The original signal is decomposed into multiple IMFs, and the MPE of each IMF is calculated. IMFs are classified into noisy and pure signals using a threshold of 0.6. The noisy signals are denoised using WTD, and the pure signals are then superimposed to complete the denoising process. The effectiveness of this method has been demonstrated using synthetic simulation signals. The denoised artificial signals achieved using this method closely match the original signals in terms of waveform, and both frequency-domain and time-domain SNRs are higher than those obtained by other methods. Additionally, the mean squared error is as low as 0.58293, showing significant advantages over Wavelet Threshold Denoising and non-optimized VMD denoising methods.
2. A flow-induced vibration model test is conducted on a hydraulic engineering project in Southwest China, and the proposed method is applied to denoise the measured vibration signals from the model test. The results indicate that the noise in the gate vibration signals is effectively removed using the proposed method. The denoising error is minimized to 1.14, which is significantly lower than that of other denoising methods, such as WTD. Additionally, the use of the MVO optimization method to optimize the VMD hyperparameters results in the shortest computation time compared to other optimization methods, demonstrating a strong advantage in computational efficiency.
3. In terms of preserving signal characteristic information, a finite element model of the flow field is established to compute and compare the frequencies from the numerical simulation with those obtained from the denoised measured signals in the model test. The first- and second-order frequencies of the measured signals are 8.2 Hz and 18.31 Hz, respectively, while the corresponding frequencies from the numerical simulation are 8.27 Hz and 18.20 Hz. The overall error between the measured and simulated frequencies is less than 1%, further confirming that the proposed joint denoising method successfully retains essential information in the vibration signals while effectively removing noise. This method is applicable for denoising measured gate vibration signals.

8. Future Research Directions

Based on the effectiveness of the proposed method, future research can be extended in the following aspects.

The first is optimization algorithm improvement. It would be valuable to explore the integration of the MVO algorithm with other global optimization algorithms, such as a Genetic Algorithm (GA) and Particle Swarm Optimization (PSO), to further enhance the parameter optimization of VMD and avoid the issue of local optima.

The second is adaptive wavelet threshold selection. In this study, a fixed wavelet threshold is used. Future research could focus on developing adaptive threshold selection methods that dynamically adjust the threshold based on signal characteristics, thereby improving the overall denoising performance.

The third is expanding application areas. While the current study primarily focuses on vibration signal processing for spillway radial gates, future work could extend the method to other complex, non-stationary signal processing scenarios, such as a rotating machinery fault diagnosis and seismic signal analysis, to validate its applicability and effectiveness in other fields.

Author Contributions: Conceptualization, X.L. and Y.L.; methodology, X.L. and X.Z.; software, X.L. and C.W.; validation, X.L. and X.Z.; formal analysis, D.Z. and X.Z.; investigation, D.Z.; resources, Y.L., D.Z. and S.T.; data curation, X.L.; writing—original draft preparation, X.L.; writing—review and editing, Y.L.; visualization, Y.L.; supervision, S.T. and Y.L.; project administration, S.T., C.W. and Y.L.; funding acquisition, S.T., Y.L. and D.Z. All authors have read and agreed to the published version of the manuscript.

Funding: This research was funded by Science and Technology Projects of CHINA HUANENG GROUP (grant No. HNKJ22-H108), Science and Technology Projects of China Power Construction Corporation Limited (grant No. DJ-ZDXM-2021-03), and the National Natural Science Foundation of China (grant No. 52179060, 52479060).

Institutional Review Board Statement: Not applicable.

Informed Consent Statement: Not applicable.

Data Availability Statement: The raw data supporting the conclusions of this article will be made available by the authors on request.

Conflicts of Interest: Authors Xiudi Lu, Shoulin Tan, and Xueyu Zheng were employed by the company Power China Guiyang Engineering Corporation Limited. The remaining authors declare that the research was conducted in the absence of any commercial or financial relationships that could be construed as a potential conflict of interest.

Nomenclature

$A_k(t)$	Instantaneous amplitude
$\varphi_k(t)$	Instantaneous phase
$\{u_k\}$	K decomposed Intrinsic Mode Functions (IMFs)
$\{w_k\}$	Central frequency components of each IMF
f	Input signal
S	Maximum scale factor
X_1	Artificial pure signal1
X_2	Artificial pure signal2
X_3	Artificial pure signal3
X_{noise}	Random white noise signal
Y	Noise-contaminated simulated signal
$[M]$	Mass matrix
$[C]$	Damping matrix
$[K]$	Stiffness matrix
$X[k]$	FFT result of the signal on the k-th frequency component
$N[k]$	FFT result of the noise on the k-th frequency component
$s[n]$	Signal value at the n-th time instant
$n[n]$	Noise value at the n-th time instant
P_s	Power of a noise-contaminated signal
P_g	Power of the denoised signal
SNR_{time}	Time-domain signal-to-noise ratio
SNR_{freq}	Frequency-domain signal-to-noise ratio
MSE	Mean squared error
K_{ij}	Variance contribution rate
k_{ij}	Distribution coefficient
NGO	Northern Goshawk Optimization
AOA	Archimedes optimization algorithm
RIME	Rime optimization algorithm
MVO	Multiverse Optimizer Algorithm
EMD	Empirical Mode Decomposition
VMD	Variational Mode Decomposition
MPE	Multiscale Permutation Entropy
WTD	Wavelet Threshold Denoising

References

1. Wang, Z.Z.; Zhang, X.C.; Liu, J.L. Research progress and development trend of large hydraulic steel gates. *J. Hydroelectr. Eng.* **2017**, *36*, 1–18. (In Chinese)
2. Han, Y.; Liu, J.; Cai, K.; Wang, Z. Topology optimization base on stability of tainter gate arm considering multi-condition. In Proceedings of the International Conference on Mathematics and Machine Learning, Nanjing, China, 24–26 November 2023; pp. 212–219. [CrossRef]
3. Han, Y.; Zhang, X.; Cai, K.; Chai, X.; Li, J.; Wang, Z. Numerical Optimization of the Dendritic Arm of a Radial Gate Based on Stability and Light Weight. *Sustainability* **2022**, *14*, 16507. [CrossRef]
4. Xu, C.; Wang, Z.; Zhang, H.; Li, H.; Li, D. Investigation on mode-coupling parametric vibrations and instability of spillway radial gates under hydrodynamic excitation. *Appl. Math. Model.* **2022**, *106*, 715–741. [CrossRef]
5. Zhang, R.; Tian, Y.H.; Li, H.L. Application of improved radar chart in the health evaluation model of hydraulic gate. *Mech. Ind.* **2022**, *23*, 24. [CrossRef]
6. Lu, Y.; Liu, Y.; Zhang, D.; Cao, Z.; Fu, X. Chaotic Characteristic Analysis of Spillway Radial Gate Vibration under Discharge Excitation. *Appl. Sci.* **2024**, *14*, 99. [CrossRef]
7. Singh, S.; Kumar, N. Combined rotor fault diagnosis in rotating machinery using empirical mode decomposition. *J. Mech. Sci. Technol.* **2014**, *28*, 4869–4876. [CrossRef]
8. Zhang, J.; Hou, G.; Wang, H.; Zhao, Y.; Huang, J.; Zhang, J.; Hou, G.; Wang, H.; Zhao, Y.; Huang, J. Operation feature extraction of flood discharge structure based on improved variational mode decomposition and variance dedication rate. *J. Vib. Control.* **2019**, *26*, 229–240. [CrossRef]
9. Pan, Q.; Zhang, L.; Dai, G.; Zhang, H. Two denoising methods by wavelet transform. *IEEE Trans. Signal Process.* **1999**, *47*, 3401–3406. [CrossRef]
10. Jin, Z.; Chen, G.; Yang, Z. Rolling Bearing Fault Diagnosis Based on WOA-VMD-MPE and MPSO-LSSVM. *Entropy* **2022**, *24*, 927. [CrossRef]
11. Zhou, J.; Xiao, M.; Niu, Y.; Ji, G. Rolling Bearing Fault Diagnosis Based on WGWOA-VMD-SVM. *Sensors* **2022**, *22*, 6281. [CrossRef]
12. Zhang, C.; Li, Z.; Ge, Y.; Liu, Q.; Suo, L.; Song, S.; Peng, T. Enhancing short-term wind speed prediction based on an outlier-robust ensemble deep random vector functional link network with AOA-optimized VMD. *Energy* **2024**, *296*, 131173. [CrossRef]
13. Wang, Q.; Hu, S.; Wang, X. Detection of incipient rotor unbalance fault based on the RIME-VMD and modified-WKN. *Sci. Rep.* **2024**, *14*, 4683. [CrossRef] [PubMed]
14. Yan, X.; Jia, M. Application of CSA-VMD and optimal scale morphological slice bispectrum in enhancing outer race fault detection of rolling element bearings. *Mech. Syst. Signal Process.* **2019**, *122*, 56–86. [CrossRef]
15. Wang, Y.; Zhang, S.; Cao, R.; Xu, D.; Fan, Y. A Rolling Bearing Fault Diagnosis Method Based on the WOA-VMD and the GAT. *Entropy* **2023**, *25*, 889. [CrossRef]
16. Gao, H.; Xu, T.; Li, R.; Cai, C. Gearbox Fault Diagnosis Based on ICEEMDAN-MPE-AWT and SE-ResNeXt50 Transfer Learning Model. *Appl. Sci.* **2024**, *14*, 2565. [CrossRef]
17. Dai, J.; Tang, J.; Shao, F.; Huang, S.; Wang, Y. Fault Diagnosis of Rolling Bearing Based on Multiscale Intrinsic Mode Function Permutation Entropy and a Stacked Sparse Denoising Autoencoder. *Appl. Sci.* **2019**, *9*, 2743. [CrossRef]
18. Liu, F.; Zhang, L.; Pang, B. Denoising Method of Discharge Guide Wall Vibration Signal Based on CEEMDAN and MPE and Its Application. *J. Zhengzhou Univ. (Eng. Sci.)* **2022**, *43*, 91–97. (In Chinese)
19. Farahmand-Tabar, S.; Babaei, M. Memory-assisted adaptive multi-verse optimizer and its application in structural shape and size optimization. *Soft Comput.* **2023**, *27*, 11505–11527. [CrossRef]
20. Chen, K.; Zhang, X.; Liu, Y.; Ma, J. An improved denoise method based on EEMD and optimal wavelet threshold for model building of OPAX. *Proc. Inst. Mech. Eng. Part D J. Automob. Eng.* **2021**, *235*, 3530–3544. [CrossRef]
21. Qiao, Y.; Li, Q.; Qian, H.; Song, X. Seismic signal denoising method based on CEEMD and improved wavelet threshold. *IOP Conf. Ser. Earth Environ. Sci.* **2021**, *671*, 012036. [CrossRef]
22. Dong, H.; Liu, S.; Liu, D.; Tao, Z.; Fang, L.; Pang, L.; Zhang, Z. Enhanced infrasound denoising for debris flow analysis: Integrating empirical mode decomposition with an improved wavelet threshold algorithm. *Measurement* **2024**, *235*, 114961. [CrossRef]
23. Wang, S.; Zhao, W.; Zhao, S.; Hao, G.; Long, F.; Su, H. Noise Reduction Analysis of Tunnel Blasting Vibration Data Based on OVMD-MPE Algorithm. *Blasting* **2023**, *40*, 166–173. (In Chinese)
24. Xu, F.; Jing, R.; Zhang, Y.; Liu, Q.; Wu, Y.A. High accuracy key feature extraction approach for the non-stationary signals measurement based on NGO-VMD noise reduction and CNN-LSTM. *Meas. Sci. Technol.* **2024**, *35*, 015031. [CrossRef]
25. Wu, S.; Xia, G.; Liu, L. A novel decomposition integration model for power coal price forecasting. *Resour. Policy* **2023**, *80*, 103259. [CrossRef]
26. Zhang, Y.; Li, C.; Lin, L.; Wang, R. Fault disgnosis of centrifugal blowers based on multi-source information fusion and ADCNN. *J. Chongqing Univ.* **2022**, *45*, 86–96. (In Chinese)
27. Li, H.; Liu, S.; Wei, B.; Huang, J.; Fu, X. Multi-point dynamic response data fusion method for a flood discharge structure based on variance dedication rate. *J. Vib. Shock.* **2015**, *34*, 181–191. (In Chinese)
28. Zhang, Z.H.; Lan, J.X.; Fan, F.; Zhi, X.D. Selection of New Type Radial Steel Gate and Analysis of Static and Dynamic Characteristics. *Int. J. Steel Struct.* **2021**, *21*, 1630–1643. [CrossRef]

29. Sun, S.; Zhang, R.; Liu, X.; Liu, C.; Wang, A. Numerical Simulation and Application of Radial Steel Gate Structure Based on Building Information Modeling under Different Opening Degrees. *Water* **2024**, *16*, 636. [CrossRef]
30. Brusewicz, K.; Sterpejkowicz-Wersocki, W.; Jankowski, R. Modal Analysis of a Steel Radial Gate Exposed to Different Water Levels. *Arch. Hydro-Eng. Environ. Mech.* **2017**, *64*, 37–47. [CrossRef]
31. Shi, S.; Han, Y.; Hu, K.; Zhou, Y.; Hu, T.; Lou, Y.; Wang, J.; Hou, T. Study on dynamic response characteristics of radial steel gate under rare earthquake considering fluid structure coupling effect. *Rev. Int. Metodos Numer. Para Calc. Diseno Ing.* **2023**, *39*, 1–15. [CrossRef]
32. Lu, X.; Liu, Y.; Lu, Y.; Fu, X. Static and Dynamic Study of Emersed Radial Gate Base on Gate-Dam System. *China Rural. Water Hydropower* **2024**, *5*, 256–263. (In Chinese)
33. Zhang, X.; Lou, S.; Chen, L.; Wang, Z.; Zhang, F. Study on Analysis Principle of Spatial System Method for a Hydraulic Steel Gate. *Sustainability* **2022**, *14*, 14804. [CrossRef]